Analysis of Dipolar and Exchange Interactions between Manganese and Tyrosine Z in the S2YZ• State of Acetate-Inhibited Photosystem II via EPR Spectral Simulations at X- and Q-Bands

ARTICLE *in* THE JOURNAL OF PHYSICAL CHEMISTRY B · SEPTEMBER 1998

Impact Factor: 3.3 · DOI: 10.1021/jp982140p

Analysis of Dipolar and Exchange Interactions between Manganese and Tyrosine Z in the $S_2Y_Z^\bullet$ State of Acetate-Inhibited Photosystem II via EPR Spectral Simulations at X- and Q-Bands

K. V. Lakshmi,[†] Sandra S. Eaton,[‡] Gareth R. Eaton,[‡] Harry A. Frank,[§] and Gary W. Brudvig*,[†]

Department of Chemistry, Yale University, New Haven, Connecticut 06520-8107, Department of Chemistry and Biochemistry, University of Denver, Denver, Colorado 80208-2436, and Department of Chemistry, University of Connecticut, Storrs, Connecticut 06269-4060

Received: May 6, 1998; In Final Form: July 22, 1998

Upon room-temperature illumination, acetate-inhibited photosystem II membranes are known to exhibit a 240 G wide X-band (∼9.5 GHz) electron paramagnetic resonance (EPR) signal at 10 K. This EPR signal arises from an interaction between the $S = 1/2$ multiline S_2 state of the tetranuclear manganese cluster and an oxidized tyrosine residue, $Y_Z^\bullet$. In the present study, the exchange and dipolar interactions between the two paramagnetic species are simulated at X- and Q-band (∼33 GHz) frequencies utilizing second-order perturbation theory. The positions and relative intensities of the hyperfine lines in the $S = 1/2$ S_2 state multiline EPR signal of the noninteracting Mn_4 cluster are accurately simulated by including g anisotropy and four sets of axially symmetric ^{55}Mn hyperfine tensors. These parameters are then used to simulate the dipolar and exchange interactions giving rise to the interacting $S_2Y_Z^\bullet$ (formerly referred to as S3) EPR signal. Relative intensities of components of the $S_2Y_Z^\bullet$ EPR spectrum, at both X- and Q-band frequencies, are best reproduced with a dipolar coupling corresponding to an interspin distance of 7.7 Å and an exchange coupling (J) of -280×10^{-4} cm^{-1}.

Introduction

During the water-oxidation chemistry in photosystem II (PS II), a tetranuclear manganese−oxo (Mn_4) cluster in the O_2-evolving complex (OEC) is sequentially oxidized in four light-driven steps. The successive formation of these intermediate oxidation states or "S states" leading to the oxidation of two molecules of water and the release of dioxygen is known as the Kok cycle.[1] The Mn_4 cluster not only acts as a charge accumulation device but is also an active participant in the water-oxidation reaction. PS II has two symmetry-related redox-active tyrosine residues in the D1 and D2 polypeptides (D1-Tyr-161, Y_Z, and D2-Tyr-160, Y_D, respectively, cyanobacterial numbering) that form the core of PS II.[2,3] Although symmetrically positioned, the two residues differ notably in their respective functions. Y_Z functions as a redox link between the water-splitting Mn_4 catalyst and a charge-separating chlorophyll moiety, P_{680}, whereas Y_D is known to undergo redox chemistry but is not directly involved in the production of dioxygen by the OEC. The two residues differ profoundly in their electron-transfer kinetics,[3] and the formation and breaking of hydrogen bonds during the redox reactions of Y_Z is taken to be indicative of protonic movement.[4,5] This has led to suggestions that Y_Z is tailored to perform proton transfer in addition to its simple redox-active role in the water-oxidation reaction of PS II, i.e., a proton-coupled electron-transfer mechanism. Direct involvement of Y_Z in water-oxidation chemistry is attractive because coupling of a proton-transfer step to the electron-transfer reaction can significantly enhance the electrochemical driving force for the process.

Recently, several metalloradical mechanistic models invoking $Y_Z^\bullet$ in the water-oxidation chemistry have been proposed via proton abstraction[6,7] or H atom abstraction.[4,8] Force et al. propose a model[7] wherein $Y_Z^\bullet$ abstracts protons from substrate water molecules bound to the Mn_4 cluster via a two-site donor−acceptor mechanism, which does not involve geometric rearrangement of $Y_Z^\bullet$. This model requires that the tyrosine residue, Y_Z, be associated with substrate bound to the Mn_4 cluster either via a direct hydrogen bond or via a hydrogen-bonded network. Babcock and co-workers propose a similar scheme[4,8] but suggest that $Y_Z^\bullet$ functions in direct H atom abstraction from substrate bound to the Mn_4 cluster via movement between two Mn-bound substrate molecules with considerable positional rearrangement of Y_Z during the donor−acceptor reactions. To elucidate the role of $Y_Z^\bullet$ in the water-oxidation reaction in PS II, it is important to determine the distance between $Y_Z^\bullet$ and the Mn_4 cluster as precisely and accurately as possible.

Rapid Mn_4 to $Y_Z^\bullet$ electron-transfer precludes stable formation of $Y_Z^\bullet$ in O_2-evolving PS II samples. However, inhibitory treatments (such as the addition of acetate) are known to block the S state cycle; room-temperature illumination of these treated PS II samples generates the $S_2Y_Z^\bullet$ (formerly known as S3) state, which can be trapped by freezing and exhibits a broadened radical EPR signal.[6,9−12] Recent electron spin echo−electron nuclear double resonance (ESE−ENDOR) data[6] and electron spin echo envelope modulation (ESEEM) studies on cyanobacterial PS II[9] indicate that the broadened radical is $Y_Z^\bullet$. Furthermore, the broad EPR line shape and enhanced spin−

* To whom correspondence should be addressed. Phone: (203) 432 5202. Fax: (203) 432 6144. E-mail: Gary.Brudvig@Yale.Edu.
[†] Yale University.
[‡] University of Denver.
[§] University of Connecticut.

S1089-5647(98)02140-3 CCC: $15.00
Published on Web 09/10/1998

lattice relaxation of $Y_Z^{\bullet}$,[12−14] along with the presence of ^{55}Mn hyperfine structure flanking the broadened radical EPR signal,[10,14,15] suggest a spin−spin interaction between $Y_Z^{\bullet}$ and the $S = 1/2$ multiline S_2 oxidation state of the Mn_4 cluster in the $S_2Y_Z^{\bullet}$ state of acetate-inhibited PS II. It has also been suggested that the broadened radical EPR signal arises from exchange and dipole interactions between two organic radicals based on a study of the $S_2Y_Z^{\bullet}$ signal in Ca^{2+}-depleted PS II membranes by analysis of the dependence of the spin echo intensity on the microwave magnetic field.[16]

Analysis of exchange and dipolar couplings between interacting spins provides valuable structural data and can be used as an effective tool to probe the geometry of the active water-oxidation site of PS II. In the present case, the $S_2Y_Z^{\bullet}$ EPR signal from acetate-treated PS II samples is ideal for evaluation of exchange and dipolar interactions because it is the only inhibited species for which the EPR signals for both the Mn_4 and $Y_Z^{\bullet}$ spins are observable. This provides the opportunity to characterize the electronic structure of each of the interacting species (Mn_4 and $Y_Z^{\bullet}$) as well as the EPR signal that results from interaction of the two spins.

Various estimates have been made of the distance between $Y_Z^{\bullet}$ and the Mn_4 cluster in the $S_2Y_Z^{\bullet}$ state of PS II. As a result of the lack of broadening in the $Y_Z^{\bullet}$ EPR signal at room temperature, Hoganson and Babcock[17] proposed a 10−20 Å distance between the two. A similar distance estimate was made by Kodera et al.[18] in an EPR study at 80 K of the magnetic relaxation of $Y_Z^{\bullet}$ in Ca^{2+}-depleted PS II. On the basis of a simple point dipole approximation, a 7 Å distance was proposed by Baumgarten et al.[19] Using a similar strategy, Nugent and co-workers estimated that $Y_Z^{\bullet}$ is significantly less than 10 Å from the Mn_4 cluster.[13] In a subsequent study, Nugent and co-workers reported EPR spectral simulations of $S_2Y_Z^{\bullet}$ signals from ammonia- and acetate-inhibited samples using a fixed distance of 9 Å.[20] Preliminary analysis of the temperature and orientation dependence of the $S_2Y_Z^{\bullet}$ signals in acetate-treated PS II by Szalai et al.[15] suggested a 6−8 Å distance between the two species. These distance estimates of 6−20 Å are currently under debate. Gilchrist et al.[6] and Force et al.[7] initially proposed that the interaction between the Mn_4 cluster and $Y_Z^{\bullet}$ is purely dipolar, yielding a distance as short as 3.5 Å between the two (assuming an $S = 1$ spin state for the Mn_4 cluster). However, the $S_2Y_Z^{\bullet}$ EPR signal in acetate-treated PS II exhibits S_2 multiline features,[10,14,15] arising from an $S = 1/2$ mixed-valence spin state of the Mn_4 cluster. Furthermore, it is unlikely that the spin−spin interaction between $Y_Z^{\bullet}$ and the S_2 state of the Mn_4 cluster would be purely dipolar if the interspin distance is as short as 3.5 Å,[6,7] because an exchange interaction is likely to be significant at such a short distance.[21,22] On the basis of more recent ^{55}Mn ENDOR experiments conducted by Peloquin et al. on the $S_2Y_Z^{\bullet}$ state, a revised Mn_4 to $Y_Z^{\bullet}$ distance of 8.6−11.5 Å is now being proposed.[23] This distance is in agreement with a recent estimate of 8−9 Å by Babcock and co-workers from simulations of the $S_2Y_Z^{\bullet}$ EPR signal.[24]

Thus, there currently is substantial uncertainty concerning the geometry of the OEC and particularly the proximity of $Y_Z^{\bullet}$ to the Mn_4 cluster. In this work, X- and Q-band EPR measurements of the $S_2Y_Z^{\bullet}$ state are presented and spectral simulations of the exchange and dipolar interactions between $Y_Z^{\bullet}$ and the S_2 state of the Mn_4 cluster at both frequencies are used to determine an accurate distance between $Y_Z^{\bullet}$ and the Mn_4 cluster in acetate-inhibited PS II. This information is important for evaluation and development of models for the mechanism of water oxidation by the OEC.

Materials and Methods

Sample Preparation. PS II membrane fragments were isolated from spinach by previously published procedures.[25] O_2-evolution rates were monitored by a Clark electrode[26] and were typically between 425 and 475 μmol of O_2 (mg of Chl)$^{-1}$ h^{-1}. Acetate-treated PS II membranes for the $S_2Y_Z^{\bullet}$ experiments were prepared as previously described by Szalai and Brudvig[10] and resuspended in a buffer containing 40 mM 2-(*N*-morpholino)-ethanesulfonic acid (MES), 0.3 M sucrose, and 500 mM sodium acetate at pH 5.5. PS II membranes used for the S_2 multiline EPR experiments were resuspended in buffer containing 15 mM sodium chloride, 20 mM MES, 5 mM $MgCl_2 \cdot 6H_2O$, 1 mM ethylenediaminetetraacetic acid (EDTA), 1 mg/mL bovine serum albumin (BSA), and 30% ethylene glycol (v/v) at pH 6.0. Phenyl-*p*-benzoquinone in dimethyl sulfoxide (DMSO) was added as an electron acceptor prior to illumination in both cases.

The S_2 state was cryotrapped by a 40 s illumination at 200 K followed by rapid freezing (5−10 s) at 77 K, in the dark. The $S_2Y_Z^{\bullet}$ state was trapped by a 10 s illumination at 298 K followed by rapid freezing at 77 K. The samples were dark-adapted prior to each illumination protocol.

EPR Spectroscopy. X-band EPR measurements were performed on a Varian E-9 spectrometer (operating at a frequency of 9.28 GHz) equipped with a TE_{102} cavity and a helium flow cryostat (Oxford Instruments). Q-band EPR measurements were performed on a Bruker ESP 300 instrument (operating at a frequency of 33.8 GHz) equipped with a ER 5106 QT low-temperature Q-band resonator and a liquid helium immersion cryostat (Oxford Instruments). Standard 4 mm quartz EPR tubes were used for the X-band measurements, and 2 mm quartz tubes (Wilmad Glass) were used for those at Q-band. All spectra reported are light-minus-dark difference spectra.

Spectral Simulations. The "split" tyrosyl radical EPR signals in Ca^{2+}-depleted PS II membranes[6,16] and in acetate-treated PS II membranes[7] have previously been analyzed as "Pake doublets". These analyses considered only the spin−spin splitting along the parallel and perpendicular axes of the dipole tensor and did not take account of the dependence of the relative intensities of the components of the spin−spin split signal when the exchange coupling is comparable to (or greater than) the difference between the energies of the interacting transitions. The current simulations include both the full orientation dependence of the spin−spin interaction and the dependence of the intensities of the signals on the energy separations between the Mn and tyrosyl transitions. MacLachlan et al.[20] used a similar approach to simulate the "split" signal for ammonia- and acetate-inhibited PS II membranes. However, in that study, the interspin distance was fixed at 9.0 Å, the Mn center was assumed to be a dimer, and no simulations of the Mn signal were attempted. In the present study, we have varied both the interspin distance and the exchange interaction to optimize the fit to the signals from both the tyrosyl radical and the Mn_4 cluster. Analysis of the signals from both halves of the interacting pair puts greater constraints on the interaction parameters than can be obtained by analysis only of the tyrosyl radical signal.

Simulation of S_2 state multiline EPR signals arising from a mixed-valence Mn_4 cluster in the O_2-evolving center of PS II requires that the hyperfine interactions of the $S = 1/2$ electron spin with four inequivalent ^{55}Mn ($I = 5/2$) nuclei be considered. However, as noted by Eaton et al.,[27] inclusion of extensive metal hyperfine interactions makes diagonalization of the Hamiltonian for a spin-coupled system such as the $S = 1/2$ Mn_4 cluster interacting with $Y_Z^{\bullet}$ very time-consuming. The feasibility of

applying a second-order perturbation theory approach to obtain dipolar and exchange couplings has been established in spin-labeled copper complexes.[27] In the present study, the *g* and *A* values for the four manganese nuclei that comprise the Mn_4 cluster were adjusted to give the best fit to the noninteracting S_2 state multiline EPR signal from PS II. These parameters were then used in second-order perturbation calculations[27] of the X- and Q-band spectra that arise from spin−spin coupling between the Mn_4 cluster and $Y_Z^\bullet$ in the $S_2Y_Z^\bullet$ state.

The S_2 state multiline powder spectra for a noninteracting $S = 1/2$ Mn_4 cluster were simulated using Fortran programs "MnSplit" and "MnSplit4". These programs are modifications of Monmer,[28] which is based on the approach used by Toy et al. and Pilbrow.[29,30] In "MnSplit", hyperfine coupling to one ^{55}Mn ($I = 5/2$) is calculated to second order and coupling to three additional equivalent ^{55}Mn is calculated to first order. In "MnSplit4", hyperfine coupling to four inequivalent ^{55}Mn is calculated to second order. Both programs include *g* and *A* anisotropy and assume coaxial orientations of the metal **g** and **A** tensors. Powder patterns are calculated by summing contributions over an octant.

The spin-coupled spectra of $S_2Y_Z^\bullet$ were calculated with "MnMeno", which is a modification of Meno.[27] The Hamiltonian includes Zeeman terms for the two $S = 1/2$ centers, hyperfine coupling to one ^{55}Mn that is treated to second order, hyperfine coupling to three additional equivalent ^{55}Mn that is treated to first order, and dipolar and exchange interactions. The exchange term in the Hamiltonian is $-J\mathbf{S}_1\cdot\mathbf{S}_2$, and thus a negative value of *J* (as is obtained in our calculations) indicates an antiferromagnetic interaction. The dipole−dipole interaction is treated as point-dipolar, with the two centers separated by a distance *r*. Interaction between the two $S = 1/2$ centers is analyzed by second-order perturbation theory. As in MnSplit and MnSplit4, the calculation in MnMeno assumes coaxial orientations of the **g** and **A** tensors for the four manganese, and these axes are denoted as X1, Y1, and Z1. The orientations within the interacting pair are defined by the following: ϵ, the angle between the interspin vector and Z1; η, the angle between the interspin vector and Y1; and a1, a2, a3, the Euler angles that relate the axes for the $Y_Z^\bullet$ **g** tensor to X1, Y1, and Z1.[27] The hyperfine tensor for $Y_Z^\bullet$ is not included in the calculation because the hyperfine couplings for $Y_Z^\bullet$ are small compared with the overall line widths. By analogy with NMR, the spin−spin interaction is viewed as an AB splitting of the transitions for the interacting $S = 1/2$ centers.[21,31] Using this notation, we refer to transitions as "inner" and "outer" lines (see Figure 4), and the transitions are labeled as "Mn_4" or "$Y_Z^\bullet$" based on the assignments in the limit as *J* tends to zero and *r* tends to infinity. The peak-to-peak line widths for the transitions can be varied independently in order to ascertain the contributions to the "inner" and "outer" lines from "Mn_4" or "$Y_Z^\bullet$" transitions. Powder patterns are calculated by summing contributions over a hemisphere. In the simulations of the $S_2Y_Z^\bullet$ spectra, the parameters for the Mn_4 cluster were held fixed at the values obtained by simulating the noninteracting S_2 state multiline EPR signal with MnSplit. In MnSplit, the perturbation treatment of the ^{55}Mn hyperfine is analogous to that in MnMeno. The *g* values for $Y_Z^\bullet$ were taken from a high-field EPR study by Un et al.[32] Thus, the adjustable parameters in the simulations were *r*, *J*, and the orientation parameters ϵ, η, a1, a2, and a3. Simulations were performed on a Gateway 2000 P5-133 IBM-compatible PC.

Results and Discussion

The $S_2Y_Z^\bullet$ interaction spectrum arises from dipolar and exchange interactions between the Mn_4 cluster and $Y_Z^\bullet$ in acetate-treated PS II membranes.[6,9,11,12,15] The spin−spin interaction between $Y_Z^\bullet$ and the S_2 oxidation state of the Mn_4 cluster ($S = 1/2$ spin state) is weak compared with the spin−spin interaction within the Mn_4 cluster, so the $S_2Y_Z^\bullet$ interaction can be viewed as a perturbation to the two centers. Thus, a starting point for the simulation of the spin-coupled spectra is to simulate the spectra of each of the noninteracting centers. We first focus on obtaining a reasonable simulation of the positions and hyperfine splittings of the Mn_4 S_2 state multiline signal. It is important to include the ^{55}Mn hyperfine splittings because the relative intensities of the "inner" and "outer" lines of the AB patterns depend on the energy difference between the interacting transitions, meaning that the appearance of the "split" signal depends not only on *J* and *D* but also on the positions of the lines in the Mn_4 S_2 state multiline signal.

Figure 1a shows an experimental X-band S_2 state multiline EPR signal from untreated PS II membranes. The X-band S_2 state multiline spectrum is centered at approximately $g = 2$ with 20 resolved EPR lines (that are detected within the *S*/*N* capabilities of this experiment), with an average hyperfine splitting of 84−86 G. The overall spectral width of the S_2 state multiline EPR signal is ∼2000 G. The hyperfine interaction between the $S = 1/2$ spin of the Mn_4 cluster and the four $I = 5/2$ spins on ^{55}Mn gives rise to the hyperfine structure in the S_2 state multiline spectrum. If *g* values or hyperfine couplings were isotropic, but there were inequivalent couplings to the four manganese nuclei, there would be 1296 hyperfine lines. Anisotropy in either *g* values or hyperfine couplings increases the theoretical number of lines in the spectrum even further. As a result of extensive overlap and inhomogeneous broadening of the peaks, far fewer than 1296 lines are resolved in the experimental spectrum. The time required for simulation of the spin-coupled spectra increases approximately linearly with the number of hyperfine lines. If a reasonable simulation of the multiline spectrum could be obtained by treating the ^{55}Mn hyperfine interactions as if there were one $I = 5/2$ of one type and three equivalent $I = 5/2$ of a second type, there would be 96 hyperfine lines, which would result in substantial savings in computational time. The simulation in Figure 1b was obtained with the program MnSplit, which includes hyperfine coupling to a unique $I = 5/2$ nucleus plus coupling to three equivalent $I = 5/2$. Comparison of the simulation (Figure 1b) with the experimental data (Figure 1a) indicates good agreement of the overall line shape, hyperfine peak positions, and intensities of the simulated spectrum. As a result of the relatively small number of resolved features in the experimental spectra and the number of adjustable parameters, comparable agreement with experimental data could be obtained with other slightly different sets of parameters (see Table 1).

S_2 state multiline EPR signals in untreated PS II membranes have previously been simulated using both perturbation theory and diagonalization approaches.[33−38] To test the sensitivity of the parameters to the computational model and to compare with prior calculations, simulations of the multiline spectrum also were performed with a program (MnSplit4) that treats each $I = 5/2$ center as inequivalent. Simulations were obtained for an alternate set of parameters (Figure 1c) and for the parameters reported by Zheng and Dismukes[33] (Figure 1d) and by Bonvoisin et al.[35] (Figure 1e). The agreement between the simulations shown in Figure 1 parts b and c and the experimental data (Figure 1a) is better than that for the simulations shown in

TABLE 1: Manganese Nuclear Hyperfine Coupling Constants and *g* Values for a Noninteracting S_2 State Multiline Signal of the Mn_4 Cluster in PS II[a]

figure	*g* values[b]	$A_x = A_y, A_z$[c]	$A_x = A_y, A_z$[c]	$A_x = A_y, A_z$[c]	$A_x = A_y, A_z$[c]	ref
1b[d]	2.04, 1.93	(1) 69.0, 87.0	(3) 84.0, 89.0			this work
1c	2.00, 1.95	(1) 92.0, 90.0	(3) 82.0, 78.0			this work
1d	2.01, 1.97	(2) 92.0, 121.0	(1) 75.0, 95.6	(1) 83.0, 75.0		33
1e	1.987	(1) 122.0	(1) 87.2	(1) 81.6	(1) 77.5	35

[a] Values of hyperfine coupling constants are given in units of 10^{-4} cm^{-1}. Simulations were calculated with Mnsplit (Figure 1b) or Mnsplit4 (Figure 1c−e). [b] *g* values are listed in the order $g_x = g_y, g_z$. If a single value is given, an isotropic *g* value was used. [c] The number of equivalent nuclei to which these coupling constants apply is shown in parentheses. A single entry indicates that an isotropic coupling was used. [d] A comparably good fit to the experimental data could be obtained with $g_x = 2.00$, $g_y = 1.95$, $g_z = 1.93$, coupling to one $I = 5/2$ with $A_x = A_y = 92.0$, $A_z = 90.0$ and coupling to three $I = 5/2$ with $A_x = A_y = 82.0$, $A_z = 78.0$. These parameters are similar to the values used for Figure 1c.

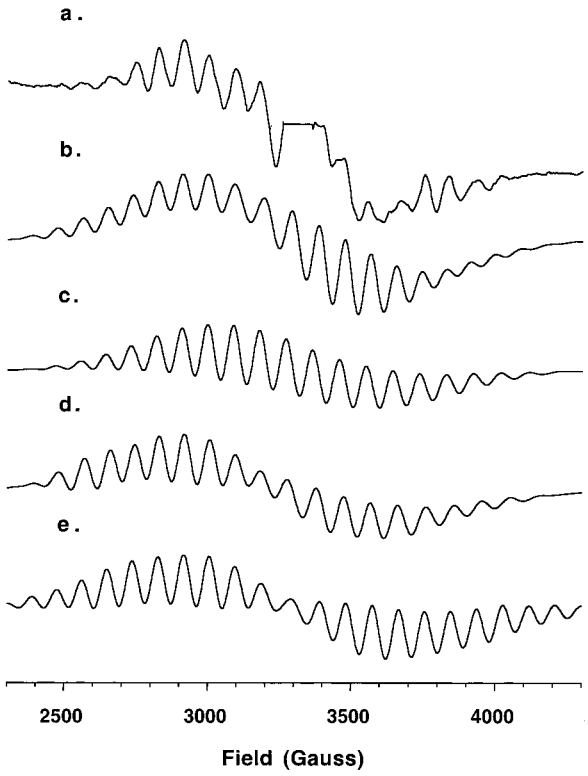

Figure 1. Comparison of experimental and simulated X-band $S = 1/2$ S_2 state multiline EPR spectra from untreated PS II membranes. (a) Experimental spectrum. There is a small contribution from the iron−quinone species, $Fe^{2+}Q_A^-$, at $g \approx 1.84$, but the presence of this species does not hinder observation of the Mn_4 multiline signal. The central (∼30 G) region of the spectrum has been edited owing to the interference from the dark-stable tyrosyl radical, $Y_D^\bullet$, in PS II. Experimental parameters: microwave frequency = 9.28 GHz; magnetic field modulation frequency = 100 kHz; modulation amplitude = 20 G; microwave power = 0.2 mW; temperature = 7 K. (b) Multiline spectrum simulated with coupling to three equivalent ^{55}Mn plus an additional inequivalent ^{55}Mn. (c) Multiline spectrum simulated with coupling to three equivalent ^{55}Mn plus an additional inequivalent ^{55}Mn, using an alternate set of parameters. (d) Multiline spectrum simulated with coupling to two equivalent ^{55}Mn plus two additional inequivalent ^{55}Mn using the parameters from Zheng and Dismukes.[33] (e) Multiline spectrum simulated with coupling to four inequivalent ^{55}Mn using the parameters from Bonvoisin et al.[35] The simulation in (b) was obtained with MnSplit and the simulations in (c−e) were obtained with MnSplit4. Hyperfine coupling constants in units of 10^{-4} cm^{-1} and *g* values are given in Table 1; microwave frequency = 9.28 GHz; peak-to-peak line width = 50 G.

Figures 1 parts d and e, especially in the wings of the spectra. The values of the hyperfine coupling constants used in the various simulations agree within approximately 10−20% (Table 1) and the hyperfine couplings to the four ^{55}Mn nuclei are of comparable magnitudes, which is in agreement with previous ENDOR results.[23,39] Given the large number of transitions that overlap in the multiline spectrum, it probably is not possible to define a unique set of hyperfine parameters based solely on the X-band data.

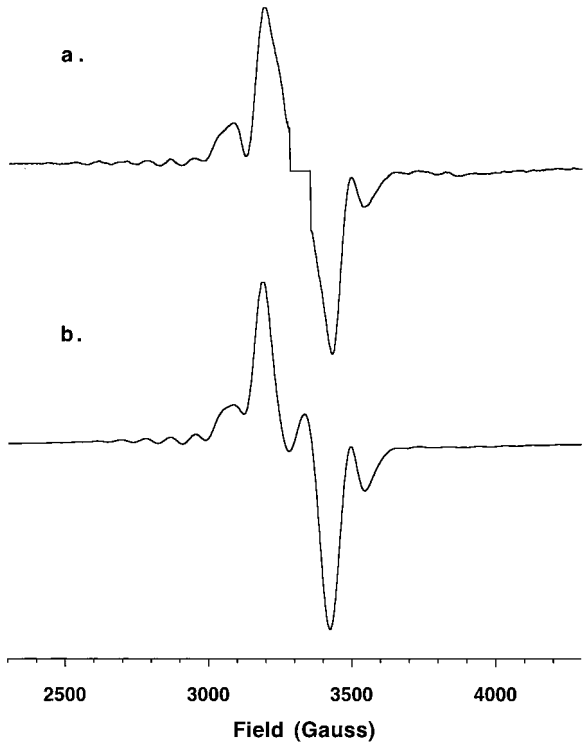

Figure 2. Comparison of experimental and simulated X-band $S_2Y_Z^\bullet$ EPR spectra in acetate-treated PS II membranes. (a) Experimental $S_2Y_Z^\bullet$ spectrum. The central (∼30 G) region of the spectrum has been edited owing to the interference from the dark-stable tyrosyl radical, $Y_D^\bullet$, in PS II. (b) Simulated $S_2Y_Z^\bullet$ spectrum for interacting $S = 1/2$ electron spins (Mn_4 and $Y_Z^\bullet$) was performed with the program MnMeno. Experimental parameters: microwave frequency = 9.28 GHz; magnetic field modulation frequency = 100 kHz; modulation amplitude = 20 G; microwave power = 20.0 mW; temperature = 7 K. Simulation parameters were the following. For Mn_4 as in Figure 1b and Table 1. For $Y_Z^\bullet$ $g_x = 2.007$; $g_y = 2.004$; $g_z = 2.002$; peak-to-peak line width = 50 G. For spin−spin interaction: $\epsilon = 0$, $\eta = 0$, $r = 7.7$ Å, and $J = -280 \times 10^{-4}$ cm^{-1}.

Having established that the present simulations compare well with those previously published and accurately simulate the hyperfine pattern of the S_2 state multiline signal in untreated PS II samples, we simulate the dipolar and exchange interactions between the $S = 1/2$ multiline S_2 state of the Mn_4 cluster and $Y_Z^\bullet$ in the $S_2Y_Z^\bullet$ state of acetate-treated PS II membranes. The dipolar and exchange couplings in the simulations are chosen to best reproduce the relative intensities of the components in the $S_2Y_Z^\bullet$ EPR spectra at both X- and Q-band. Figure 2 parts a and b show experimental and simulated X-band $S_2Y_Z^\bullet$ spectra from acetate-treated PS II membranes. The experimental X-band spectrum (Figure 2a) of the $S_2Y_Z^\bullet$ state of acetate-treated

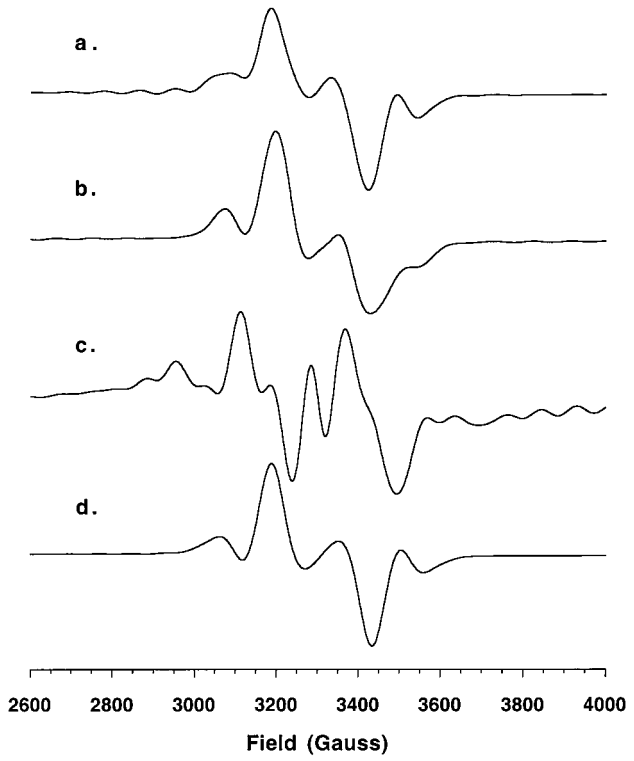

Figure 3. Demonstration of the effects on simulated $S_2Y_Z^\bullet$ EPR spectral line shapes of reversing the sign of J and of varying the dipolar and exchange couplings. $S_2Y_Z^\bullet$ simulation obtained (a) with $r = 7.7$ Å and $J = -275 \times 10^{-4}$ cm^{-1}, (b) with $r = 7.7$ Å and $J = +275 \times 10^{-4}$ cm^{-1}, (c) with a dominant dipolar interaction corresponding to a short interspin distance of 4.5 Å and a weak exchange coupling of -100×10^{-4} cm^{-1}, and (d) with a weaker dipolar interaction ($r = 40$ Å) with a stronger exchange interaction of -300×10^{-4} cm^{-1}. Simulation parameters, except for r and J, are the same as in Figure 2b.

PS II membranes exhibits broad "split" features that span from about 3000 to 3600 G (the main "split" peaks as well as the satellites) and multiline features that arise from the hyperfine couplings in the Mn_4 cluster that span ~2000 G. The spectrum in Figure 2a was acquired at 7 K and is in the static limit; thus, there is no contribution from relaxation effects, which cause averaging of the exchange and dipolar couplings at higher temperatures.[14,15] The multiline signals are due to the S_2 state in $S_2Y_Z^\bullet$ and not from residual uninhibited Mn_4 centers as evidenced by their shift of about 40 G relative to the hyperfine peaks in the noninteracting S_2 state multiline EPR signal.[14] The ^{55}Mn hyperfine peaks in the S_2 state from untreated PS II membranes are very similar to those seen in $S_2Y_Z^\bullet$ samples quenched with nitric oxide (S_2Y_Z−NO); nitric oxide binds to $Y_Z^\bullet$ to form a diamagnetic species, which uncouples the two interacting spins.[40] This similarity indicates that the electron−nuclear couplings within the Mn_4 cluster are not significantly perturbed when acetate is added to inhibit O_2 evolution in PS II and allow accumulation of the $S_2Y_Z^\bullet$ state. Thus, it is reasonable to use the same parameters for the Mn_4 cluster in the simulation of the interacting $S_2Y_Z^\bullet$ spectra as were used for the noninteracting S_2 multiline spectra (Figure 1b). There is excellent agreement between the experimental and simulated $S_2Y_Z^\bullet$ spectra for the intensities and positions of the central "split" features and of the multiline signals. These simulations were obtained with an interspin distance of 7.7 Å and an exchange coupling, J, of -280×10^{-4} cm^{-1}.

The effects on the simulated $S_2Y_Z^\bullet$ spectral line shapes due to reversing the sign of the exchange coupling (J) were examined. Figure 3a shows a $S_2Y_Z^\bullet$ simulation obtained with $J = -275 \times 10^{-4}$ cm^{-1}, while that in Figure 3b was obtained with $J = +275 \times 10^{-4}$ cm^{-1}. The dipolar coupling and relative orientations of the dipolar vector were held constant. Comparison of the simulations in Figure 3 parts a and b shows that the simulations are very sensitive to the sign of J. Variation of r and the orientation of the dipolar vector did not produce a simulation with $J > 0$ that fit the experimental data as well as the simulation shown in Figure 2b, for which $J < 0$. The negative sign of J indicates that the spins are antiferromagnetically coupled.

The central features of the experimental and simulated $S_2Y_Z^\bullet$ EPR signals in acetate-treated PS II exhibit a typical AB splitting pattern, as expected for two weakly exchange-coupled $S = 1/2$ centers with similar resonant frequencies (discussed below). The splitting is a combination of dipolar and exchange contributions. Because of the small g anisotropy for $Y_Z^\bullet$, the simulations are relatively insensitive to variation of the angles that define the orientation of the axes for $Y_Z^\bullet$ relative to the axes for the Mn_4 cluster. The simulation is also insensitive to η, the angle between the projection of the dipolar vector and Y1, the y axis of the Mn_4 cluster, because the parameters for the Mn_4 cluster are axial. Although the relative intensities of the "split" signals are not highly sensitive to ϵ, the angle between the dipolar vector and Z1 (the z axis of the Mn_4 cluster), the hyperfine peak positions in the $S_2Y_Z^\bullet$ simulations are sensitive to this angle; values of ϵ from 0 to 30° gave good agreement with the experimental spectrum. However, the splittings as well as the relative intensities of the "split" features are most sensitive to the exchange interaction, J, and the interspin distance, r, which permits us to simulate the spectra with a relatively narrow range of values of r and J (the estimated uncertainty in r is ±0.5 Å, and that in J is $\pm 10 \times 10^{-4}$ cm^{-1}).

Figure 3 parts c and d demonstrate the effects of predominantly dipolar or exchange couplings on the $S_2Y_Z^\bullet$ simulations. A purely dipolar interaction ($r = 4.5$ Å, Figure 3c) yields a spectrum with a larger splitting and relative intensities of the main "split" peaks and "satellites" that do not fit with experiment. A much weaker dipolar interaction ($r = 40$ Å) and a stronger exchange interaction, $J = -300 \times 10^{-4}$ cm^{-1}, yield a simulation (Figure 3d) that bears some resemblance to the experimental $S_2Y_Z^\bullet$ spectrum in acetate-inhibited PS II (Figure 2a), but the relative amplitudes of the spectral components and the spacing between the lowest and highest field components of the "split" spectrum do not agree with experiment as well as the simulation in Figure 3a. The greater similarity between the simulations in Figure 3 parts a and d than between those of Figure 3 parts a and c indicates that the spin−spin interaction between the S_2 state of the Mn_4 cluster and $Y_Z^\bullet$ is dominated by exchange. However, the relative intensities of the spectral components could not be simulated with exclusively an exchange interaction.

Because exchange dominates the spin−spin interaction, the "split" spectrum can be understood by analogy with NMR AB splitting patterns.[21,31] In the $S_2Y_Z^\bullet$ spin system, there is an AB splitting pattern due to interaction of each hyperfine component of the spectrum of the Mn_4 cluster with the $Y_Z^\bullet$ signal. The observed and calculated spectra result from the superposition of these AB patterns for all possible orientations of the spin-coupled pair with respect to the external magnetic field. For ^{55}Mn hyperfine components with resonance at a lower magnetic field than the $Y_Z^\bullet$ signal, the "inner" lines of the AB pattern for $Y_Z^\bullet$ (i_1, Figure 4a) are shifted to lower field than the noninteracting position and the less intense "outer" lines for $Y_Z^\bullet$ (o_1, Figure 4a) are shifted to higher field. Similarly, for ^{55}Mn

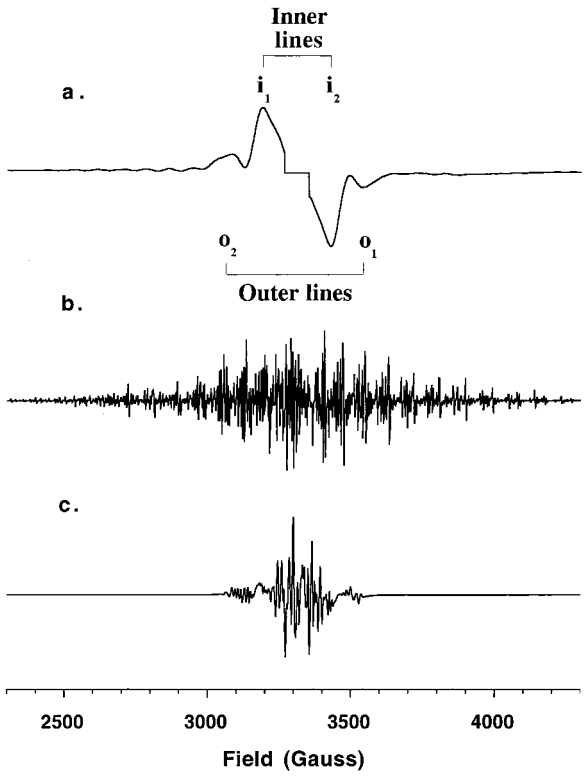

Figure 4. Visualization of the contributions predominantly from the S_2 multiline or $Y_Z^\bullet$ resonances to the interacting $S_2Y_Z^\bullet$ EPR spectrum in acetate-treated PS II membranes at X-band. (a) Experimental $S_2Y_Z^\bullet$ spectrum from acetate-treated PS II (same data as in Figure 1a). The peaks labeled i_1 and o_1 are the inner and outer $Y_Z^\bullet$ lines, respectively, due to interaction with ^{55}Mn hyperfine components at lower magnetic fields. The peaks labeled i_2 and o_2 are the inner and outer $Y_Z^\bullet$ lines, respectively, due to interaction with ^{55}Mn hyperfine components at higher magnetic fields. (b, c) Simulated $S_2Y_Z^\bullet$ spectra in which the line widths of the transitions that are predominantly Mn_4 (b) or $Y_Z^\bullet$ (c) were set to 3 G to highlight them. Simulation parameters, except for line widths, are the same as in Figure 2b.

hyperfine components with resonance at a higher magnetic field, the $Y_Z^\bullet$ "inner" and "outer" lines (i_2, o_2, Figure 4a) are shifted to higher field and lower field, respectively, relative to the noninteracting signal.

The spin−spin interaction causes each transition in the AB pattern to involve a combination of Mn_4 and $Y_Z^\bullet$ contributions; however, the spin−spin interaction for this system is small enough that it is convenient to label transitions based on the contributions in the limit as J tends to zero and r tends to infinity. In Figure 4b, the line widths for the transitions that are predominantly Mn_4 were decreased to 3 G and the line widths for transitions that are predominantly $Y_Z^\bullet$ were held at 50 G. The use of a very narrow line width for one type of transition makes these transitions readily distinguishable and demonstrates that transitions that are largely Mn_4 in character extend for more than 2000 G. In Figure 4c, the line widths for the predominantly $Y_Z^\bullet$ transitions were decreased to 3 G and the line widths for the predominantly Mn_4 transitions were held at 50 G. This simulation shows that the transitions that are predominantly $Y_Z^\bullet$ contribute spectral intensity only in the region of the "split" signal. When the line widths of the Mn_4 and $Y_Z^\bullet$ signals are comparable, as in Figure 2b, the predominantly $Y_Z^\bullet$ transitions dominate the center of the spectrum, although there are less intense underlying contributions from the predominantly Mn_4 transitions. The underlying Mn_4 transitions contribute about 15−20% to the signal intensity near $g = 2$, although their contribution is larger toward the wings of the $S_2Y_Z^\bullet$ spectrum. These comparisons support the earlier proposal, based on EPR and ESEEM data,[7] that the underlying contributions from the multiline signal (the Mn_4 transitions) do not contribute substantially to the "satellite" peaks in the X-band spectrum of $S_2Y_Z^\bullet$ in acetate-treated PS II membranes.

Figure 5 shows a comparison of the low- and high-field portions of experimental and simulated X-band S_2 state multiline signals in PS II membranes. Figure 5 parts a and e and Figure 5 parts b and f show the experimental and simulated $S_2Y_Z^\bullet$ spectra, respectively (with interacting Mn_4 and $Y_Z^\bullet$ spins). Figure 5c shows the low-field region of a simulation of the S_2 multiline spectrum from an untreated (noninteracting) sample. Figure 5d (from Szalai and Brudvig[40]) shows the low-field portion of the spectrum from an acetate-inhibited PS II sample prepared in the S_2Y_Z-NO state in which binding of nitric oxide to $Y_Z^\bullet$ yields a noninteracting S_2 state. The magnitude of the hyperfine splittings in all four multiline signals (Figure 5a−d) does not change in the interacting ($S_2Y_Z^\bullet$) versus noninteracting (untreated S_2 or S_2Y_Z-NO) cases. However, comparison of the hyperfine peak positions in the four spectra indicates that the hyperfine peaks from Mn_4 in the $S_2Y_Z^\bullet$ state exhibit shifts of ∼40 G due to spin−spin interactions (dipolar and exchange) with the $Y_Z^\bullet$ radical. In the AB patterns for the Mn_4 lines, the "inner" lines are more intense than the "outer" lines and, therefore, dominate the spectra, except in the wings. For the Mn_4 lines in the low-field portion of the spectrum, all of the transitions for $Y_Z^\bullet$ occur at higher field and so the Mn_4 "inner" lines are shifted to higher field. As marked on the spectrum in Figure 4a, the "inner" lines of the "split" signal are shifted by about 115 ± 5 G from the position of the noninteracting signal. The shift of the Mn_4 "inner" lines will be slightly different for each ^{55}Mn hyperfine line, but will be similar to that for the "inner" $Y_Z^\bullet$ lines. As a result of the large number of hyperfine lines in the Mn_4 multiline spectrum, a shift of about 40 G would be difficult to distinguish from a shift by 40 G plus the apparent hyperfine splitting of about 85 G. We, therefore, propose that the apparent shift of about 40 G is actually a shift of about 125 G, which is a reasonable shift for the Mn_4 "inner" lines.

Shown in Figure 6 parts a and b are experimental and simulated $S_2Y_Z^\bullet$ spectra in acetate-treated PS II samples at Q-band. The broad "split" signals centered at $g = 2$ are a result of the interaction between the Mn_4 cluster and $Y_Z^\bullet$ in the $S_2Y_Z^\bullet$ state of PS II. The $S_2Y_Z^\bullet$ Q-band simulation (Figure 6b) utilizes the parameters obtained in the best fit of the X-band $S_2Y_Z^\bullet$ spectrum (Figure 2b). The experimental and simulated Q-band spectra in Figure 6 parts a and b are in excellent agreement with each other. There is an asymmetric distribution of spectral intensities about $g = 2$ because the small difference in g values of the two spins has a more pronounced effect at the higher magnetic field for the Q-band measurements. Although the simulation predicts the presence of S_2 multiline features in the $S_2Y_Z^\bullet$ interaction spectrum, these are not observed in the experimental spectra. This is most likely due to S/N limitations of the Q-band measurements. Alternatively, the anisotropy of g values or inequivalence of hyperfine coupling to Mn nuclei with different g values may make the multiline signal less well-resolved at Q-band than at X-band. The line widths for the "split" signal are approximately the same at Q-band as those at X-band. The apparent line widths for these transitions are due to a combination of unresolved hyperfine coupling for the tyrosyl signal, the orientation dependence of the spin−spin interaction, and distributions in J and/or r. These contributions are not expected to be frequency dependent.

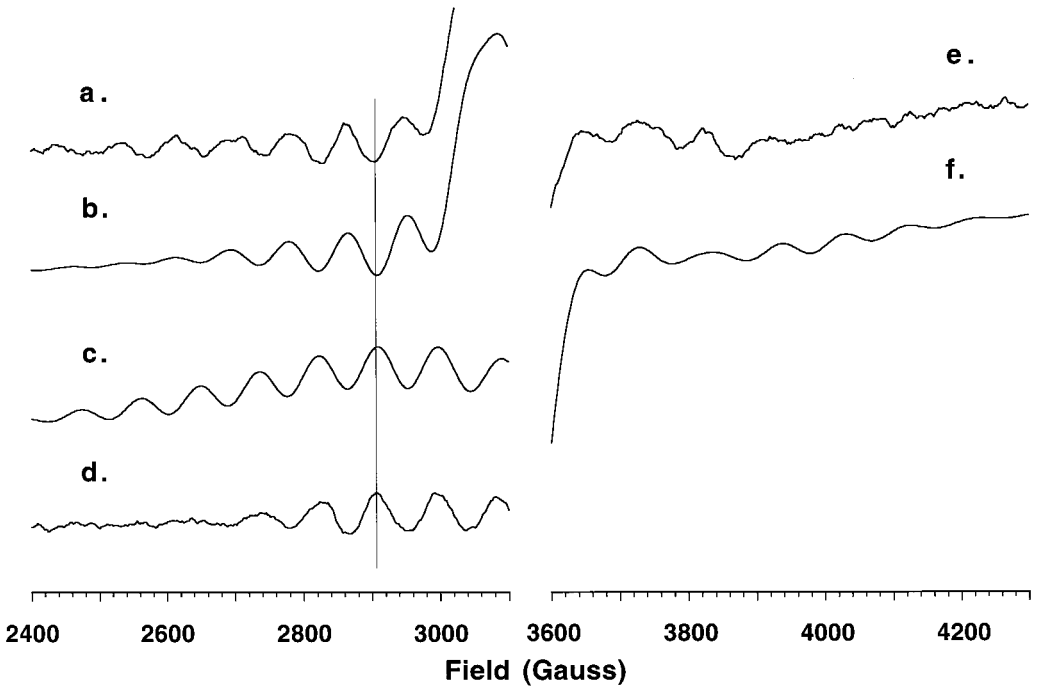

Figure 5. Comparison of the low- and high-field portions of the X-band S_2 multiline EPR signals in the interacting $S_2Y_Z^\bullet$ state with the simulated spectrum and with the low-field portions of the noninteracting S_2 state in untreated membranes and the $S_2Y_Z^\bullet$ state quenched with nitric oxide (S_2Y_Z−NO) in acetate-treated PS II membranes. (a, e) Experimental $S_2Y_Z^\bullet$ spectrum from acetate-treated PS II membranes (expansion of the spectrum in Figure 2a); (b, f) simulated $S_2Y_Z^\bullet$ spectrum (same as in Figure 2b); (c) simulated noninteracting S_2 spectrum in untreated PS II membranes (same as in Figure 1b), and (d) experimental S_2Y_Z−NO spectrum from acetate-treated PS II membranes (from Szalai and Brudvig[40]). Experimental and simulation parameters for the $S_2Y_Z^\bullet$ spectra are the same as in Figure 2. Experimental parameters for the S_2Y_Z−NO spectrum are as in Szalai and Brudvig.[40] Simulation parameters for the S_2 spectrum are the same as in Figure 1b.

The simulations of the Q-band spectra of $S_2Y_Z^\bullet$ in Figure 6c were obtained by narrowing the line widths for the transitions that are nominally identified as Mn_4 transitions. Analogously, the simulation in Figure 6d was obtained by narrowing the line widths for the transitions that are predominantly $Y_Z^\bullet$. As at X-band, this labeling of the transitions is based on the assignments of the transitions in the limit of negligible spin−spin interaction. The actual transitions contain contributions from both spins. Even so, the spectra in Figure 6 help to visualize the fact that the transitions that are largely Mn_4 are spread over a wide range of fields and the transitions that are largely $Y_Z^\bullet$ are limited to the central portion of the spectrum, analogous to the observations at X-band.

Conclusions

Simulations of the S_2 state multiline X-band EPR signal of the Mn_4 cluster based on a (1 + 3) model for the ^{55}Mn hyperfine couplings are in good agreement with the experimental data and with previously published simulations of the S_2 state multiline EPR signal.[33,35] These ^{55}Mn hyperfine couplings were then used to simulate the exchange and dipolar interactions giving rise to the $S_2Y_Z^\bullet$ EPR signal for acetate-inhibited PS II membranes. The simulated spectra are in good agreement with the experimental EPR signals at both X- and Q-bands.

The intensities and positions of both the central "split" features as well as the multiline signals in the experimental and simulated $S_2Y_Z^\bullet$ signals are best reproduced by an interspin distance of 7.7 Å and an antiferromagnetic exchange coupling of -280×10^{-4} cm^{-1}. These parameters are in good agreement with previous temperature[14,15] and orientation dependence data[41] for these signals, which indicate weak exchange and dipolar couplings between the Mn_4 and $Y_Z^\bullet$ spins. The $S_2Y_Z^\bullet$ EPR signals exhibit typical AB splitting patterns. The spin−spin interaction results in transitions that have contributions from both Mn_4 and $Y_Z^\bullet$. For $S_2Y_Z^\bullet$, the spin−spin interaction is weak enough that it is useful to identify transitions based on the assignment in the limit where J tends to zero and r tends to infinity. The "split" signal, including the "satellite" lines, is dominated by transitions that are largely $Y_Z^\bullet$, with weaker underlying lines that are largely Mn_4 transitions. The transitions that are largely Mn_4 dominate the multiline portion of the spectrum. Comparison of the multiline signals from acetate-inhibited PS II in the $S_2Y_Z^\bullet$ state (interacting spins) with those from the S_2Y_Z−NO state[40] (noninteracting spins) and comparison with the shifts in the $Y_Z^\bullet$ lines indicates that the Mn_4 hyperfine components are shifted by about 125 G due to the spin−spin interaction.

It had been suggested that it was not possible for the extra "satellite" structures in the "split" signal to arise from broadening of the $Y_Z^\bullet$ signal due to an isotropic exchange interaction with an $S = 1/2$ state of the Mn cluster.[7] Consequently, it was proposed that the interaction was purely dipolar and that the "split" peaks were the perpendicular edges of a dipolar Pake pattern, while the satellites correspond to the parallel edges. In light of the current simulations as well as revised ones from Peloquin et al.,[23] this appears not to be the case. The central "split" features and satellite peaks in the acetate-treated $S_2Y_Z^\bullet$ spectrum are a result of the $S_2Y_Z^\bullet$ spin−spin interactions (both dipolar and exchange) and contain contributions from both the S_2 state of the Mn_4 cluster and the $Y_Z^\bullet$ spins. We conclude that the resemblance of the $S_2Y_Z^\bullet$ ESEEM signal to an anisotropic dipolar Pake pattern is coincidental. The $S_2Y_Z^\bullet$ simulations for interacting spins in the present study also provide unequivocal evidence that the $S_2Y_Z^\bullet$ experimental spectrum is indeed a result of interactions between the $S = 1/2$ multiline S_2 oxidation state of the Mn_4 cluster and $Y_Z^\bullet$.

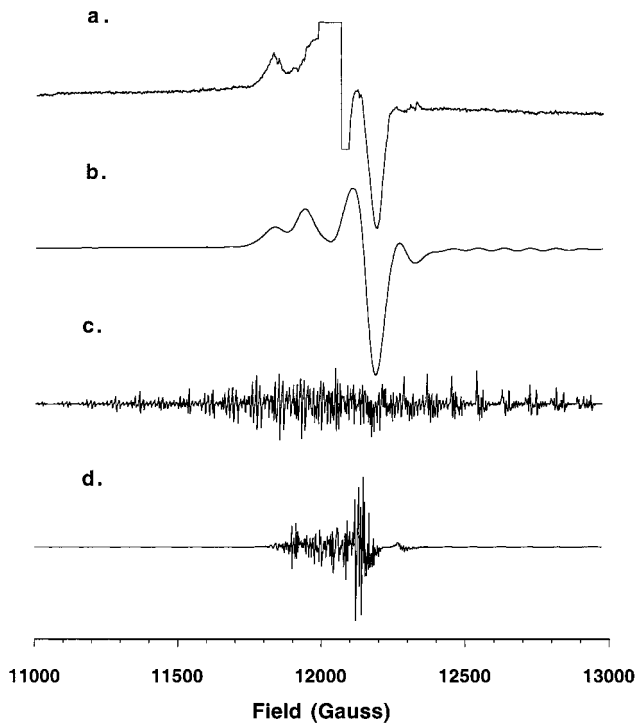

Figure 6. Comparison of Q-band experimental and simulated $S_2Y_Z^\bullet$ EPR spectra in acetate-treated PS II membranes. (a) Experimental $S_2Y_Z^\bullet$ spectrum in acetate-treated PS II. The central (~100 G) region of the spectrum has been edited owing to the interference from the dark-stable tyrosyl radical, $Y_D^\bullet$, in PS II. (b) Simulated $S_2Y_Z^\bullet$ spectra in acetate-treated PS II membranes. (c, d) Simulated $S_2Y_Z^\bullet$ spectra in which the line widths of the transitions that are predominantly Mn_4 (c) or $Y_Z^\bullet$ (d) were set to 3 G to highlight them. Experimental parameters: microwave frequency = 33.8 GHz; magnetic field modulation frequency = 100 kHz; modulation amplitude = 20 G; microwave power = 8.0 mW; temperature = 9 K. The simulation parameters in (b) are the same as in Figure 2b except that the microwave frequency = 33.8 GHz. The simulation parameters in (c) and (d), except for line widths, are the same as in (b).

The value of J obtained in the simulations (-280×10^{-4} cm^{-1}) is similar to that obtained by MacLachlan et al.[20] for acetate-treated PS II membranes ($|J| = 250 \times 10^{-4}$ cm^{-1}) by simulation only of the "split" tyrosyl signal, to the revised value obtained by Peloquin et al.[23] ($J = -850$ MHz $= -280 \times 10^{-4}$ cm^{-1}) by analysis of ENDOR data for acetate-inhibited PS II, and to that obtained by Astashkin et al.[16] for Ca^{2+}-depleted PS II membranes ($|J| = 30$ mT $\approx 280 \times 10^{-4}$ cm^{-1}) by analysis of the dependence of spin echo intensity on a microwave magnetic field with the assumption that the "split" signal is due to interaction with the Mn_4 cluster. A value of J of this magnitude indicates that there is a through-bond pathway between the tyrosyl radical and one or more of the Mn in the cluster. Such a pathway could include one or more hydrogen bonds.

The distance of 7.7 Å determined in the present study by using a point dipole approximation is an effective distance between $Y_Z^\bullet$ and the electron spin on the Mn_4 cluster. The necessity of including hyperfine couplings of comparable magnitudes for each of the four ^{55}Mn, based on previous EPR simulations and ESE-ENDOR studies, indicates that there is significant electron spin density on each of the four ^{55}Mn atoms in the Mn_4 cluster. In addition, the spin on $Y_Z^\bullet$ is distributed over the aromatic ring as determined by ENDOR measurements.[5] Therefore, modeling of the distributed spin densities on the Mn_4 cluster and $Y_Z^\bullet$ is required to relate the effective distance obtained from the EPR spectral simulations to structural models of the OEC. Nonetheless, it is clear that $Y_Z^\bullet$ is close enough to the Mn_4 cluster to be within hydrogen abstraction distance of one of the Mn-bound substrate molecules, either via a direct hydrogen bond or via a hydrogen-bonded network where proton transfer from the substrate water molecules on the Mn_4 cluster to $Y_Z^\bullet$ is mediated by either charged amino acid residues or water molecules.

Acknowledgment. The authors acknowledge Ruel Desamero and James Bautista (at the University of Connecticut) for their assistance in setting up the Q-band EPR instrument. We also thank Dr. Veronika Szalai for critical reading of the manuscript and Drs. R. David Britt and Gerald Babcock for providing manuscripts prior to publication. This work was supported by Grants GM32715 and GM36442 (Yale), GM21156 (Denver), and GM30353 (Storrs) from the National Institutes of Health and the University of Connecticut Research Foundation.

References and Notes

(1) Kok, B.; Forbush, B.; McGloin, M. *Photochem. Photobiol.* **1970**, *11*, 457−475.
(2) Michel, H.; Deisenhofer, J. *Biochemistry* **1988**, *27*, 1−7.
(3) Debus, R. J. *Biochim. Biophys. Acta* **1992**, *1102*, 269−352.
(4) Hoganson, C. W.; Lydakis-Simantiris, N.; Tang, X.-S.; Tommos, C.; Warncke, K.; Babcock, G. T.; Diner, B. A.; McCracken, J.; Styring, S. *Photosynth. Res.* **1995**, *46*, 177−184.
(5) Tommos, C.; Tang, X.-S.; Warncke, K.; Hoganson, C. W.; Styring, S.; McCracken, J.; Diner, B. A.; Babcock, G. T. *J. Am. Chem. Soc.* **1995**, *117*, 10325−10335.
(6) Gilchrist, M. L.; Ball, J. A.; Randall, D. W.; Britt, R. D. *Proc. Natl. Acad. Sci. U.S.A.* **1995**, *92*, 9545−9549.
(7) Force, D. A.; Randall, D. W.; Britt, R. D. *Biochemistry* **1997**, *36*, 12062−12070.
(8) Hoganson, C. W.; Babcock, G. T. *Science* **1997**, *277*, 1953−1956.
(9) Tang, X.-S.; Randall, D. W.; Force, D. A.; Diner, B. A.; Britt, R. D. *J. Am. Chem. Soc.* **1996**, *118*, 7638−7639.
(10) Szalai, V. A.; Brudvig, G. W. *Biochemistry* **1996**, *35*, 1946−1953.
(11) Boussac, A.; Rutherford, A. W. *Biochemistry* **1988**, *27*, 3476−3483.
(12) MacLachlan, D. J.; Nugent, J. H. A. *Biochemistry* **1993**, *32*, 9772−9780.
(13) Hallahan, B. J.; Nugent, J. H. A.; Warden, J. T.; Evans, M. C. W. *Biochemistry* **1992**, *31*, 4562−4573.
(14) Szalai, V. A.; Kühne, H.; Lakshmi, K. V.; Brudvig, G. W. *Biochemistry*, in press.
(15) Szalai, V. A.; Kühne, H.; Lakshmi, K. V.; Eaton, G. R.; Eaton, S. S.; Brudvig, G. W. *Biophys. J.* **1998**, *74*, A75.
(16) Astashkin, A. V.; Mino, H.; Kawamori, A.; Ono, T.-A. *Chem. Phys. Lett.* **1997**, *272*, 506−516.
(17) Hoganson, C. W.; Babcock, G. T. *Biochemistry* **1988**, *27*, 5848−5855.
(18) Kodera, Y.; Hara, H.; Astashkin, A. V.; Kawamori, A.; Ono, T.-A. *Biochim. Biophys. Acta* **1995**, *1232*, 43−51.
(19) Baumgarten, M.; Philo, J. S.; Dismukes, G. C. *Biochemistry* **1990**, *29*, 10814−10822.
(20) MacLachlan, D. J.; Nugent, J. H. A.; Warden, J. T.; Evans, M. C. W. *Biochim. Biophys. Acta* **1994**, *1188*, 325−334.
(21) Eaton, S. S.; Eaton, G. R. *Acc. Chem. Res.* **1988**, *21*, 107−113.
(22) Coffman, R. E.; Buettner, G. R. *J. Phys. Chem.* **1979**, *83*, 2387−2392.
(23) Peloquin, J. M.; Campbell, K. A.; Britt, R. D. *J. Am. Chem. Soc.* **1998**, *120*, 6840−6841.
(24) Dorlet, P.; Di Valentin, M.; Babcock, G. T.; McCracken, J. L. *J. Phys. Chem.*, in press.
(25) Berthold, D. A.; Babcock, G. T.; Yocum, C. F. *FEBS Lett.* **1981**, *134*, 231−234.
(26) Beck, W. F.; de Paula, J. C.; Brudvig, G. W. *Biochemistry* **1985**, *24*, 3035−3043.
(27) Eaton, S. S.; More, K. M.; Sawant, B. M.; Boymel, P. M.; Eaton, G. R. *J. Magn. Reson.* **1983**, *52*, 435−449.
(28) Rakowsky, M. H.; More, K. M.; Kulikov, A. V.; Eaton, G. R.; Eaton, S. S. *J. Am. Chem. Soc.* **1995**, *117*, 2049−2058.
(29) Toy, A. D.; Chaston, S. H. H.; Pilbrow, J. R.; Smith, T. D. *Inorg. Chem.* **1971**, *10*, 2219−2225.
(30) Pilbrow, J. R. *Mol. Phys.* **1969**, *16*, 307−309.

(31) Eaton, G. R.; Eaton, S. S. *Biol. Magn. Reson.* **1989**, *8*, 339−397.
(32) Un, S.; Tang, X.-S.; Diner, B. A. *Biochemistry* **1996**, *35*, 679−684.
(33) Zheng, M.; Dismukes, G. C. *Inorg. Chem.* **1996**, *35*, 3307−3319.
(34) Åhrling, K. A.; Pace, R. J. *Biophys. J.* **1995**, *68*, 2081−2090.
(35) Bonvoisin, J.; Blondin, G.; Girerd, J.-J.; Zimmerman, J.-L. *Biophys. J.* **1992**, *61*, 1076−1086.
(36) Haddy, A.; Waldo, G. S.; Sands, R. H.; Penner-Hahn, J. E. *Inorg. Chem.* **1994**, *33*, 2677−2682.
(37) Kusunoki, M. *Chem. Phys. Lett.* **1992**, *197*, 108−116.
(38) Hansson, Ö.; Aasa, R.; Vänngård, T. *Biophys. J.* **1987**, *51*, 825−832.
(39) Randall, D. W.; Sturgeon, B. E.; Ball, J. A.; Lorigan, G. A.; Chan, M. K.; Klein, M. P.; Armstrong, W. H.; Britt, R. D. *J. Am. Chem. Soc.* **1995**, *117*, 11780−11789.
(40) Szalai, V. A.; Brudvig, G. W. *Biochemistry* **1996**, *35*, 15080−15087.
(41) Lakshmi, K. V.; Brudvig, G. W. Unpublished data.